Hydraulic fractures from non-uniform perforation cluster spacing: Laboratory study on gelatin and data-driven modeling

Andreas Michael[1,*]

[1]Louisiana State University, Craft & Hawkins Department of Petroleum Engineering, Baton Rouge, LA, USA

Abstract. Hydraulic fracture treatments in horizontal wells involve complexities contemporary analytical and numerical models do not incorporate. Interactions between simultaneously propagating fractures affects neighboring fractures making them grow dissimilarly to each other. This leads to a non-homogeneous fracture geometry, which in many instances results to ineffective or prematurely terminated fractures and therefore sub-optimal economic performance. This project involves the creation of a probabilistic predictive model (PPM), which incorporates empirical inputs from laboratory-scale experimental tests. Random probabilistic distributions are biased statistically in order to generate profiles that match the experimental results. The PPM developed is using Monte Carlo simulation to give a likely final multi-frac geometry.

1 Introduction

Throughout the years, several attempts were made to optimize hydraulic fracture treatments. Non-uniform perforation cluster spacing has been proposed by numerical simulations [1] as a method for enhancing multiple fracture (multi-frac) growth homogeneity. Achieving a homogeneous multi-frac geometry is paramount to the economic performance of a hydraulic fracture stimulation treatment in a horizontal well.

Understanding how non-uniform perforation cluster spacing influences hydraulic fracture treatments within a single-stage and to what extend is the main objective of this study. The main dependent variable is multi-frac growth geometry, which is used in the oilfield for estimating the stimulated reservoir volume (SRV) and from there evaluating the net present value (NPV) of the overall stimulation treatment. Dominant fracture creation and inactive perforations are also discussed.

1.1 Fracture Treatments in Horizontal Wellbores

The industry has spent decades developing a reservoir stimulation technique based on the idea of creating a network of cracks that enable reservoir fluids to flow out of the rock. This became known as hydraulic fracturing; a process used today by virtually all wells for the production of commercial hydrocarbon quantities from unconventional reservoirs. Hydraulic fracturing operations combined with horizontal wellbores are key in producing hydrocarbons profitably from low permeability formations, such as shale [2].

A typical fracture treatment in a horizontal well (Fig. 1) is comprised of a number of stages. Each stage consists of a number of perforation clusters; usually from three to six each with multiple of perforations per cluster. Out of all perforations in each cluster "active" perforations are the ones generating fractures.

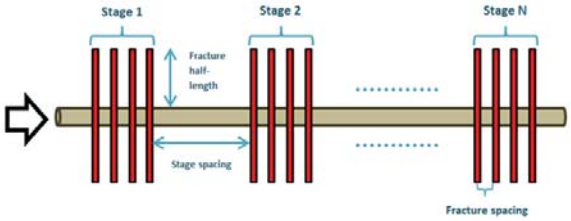

Fig. 1. Schematic of a typical multi-stage fracture treatment in a horizontal well (from [3]).

1.2 Motivation

The creation of a fracture generates perturbations in the surrounding stress field, which affects the propagation of other fractures making them grow dissimilarly and terminate early. Fig. 2a shows the impact on multi-frac growth for three, five and six perforation clusters.

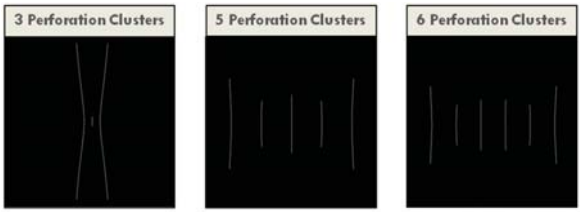

Fig. 2a. Non-homogeneous multiple fracture propagation geometries. Those simulations were performed using *JOINTS 2.3* geomechanics software [4]. One active perforation per cluster is assumed. The horizontal well (not shown) is has its "heel" on the left and "toe" to the right (modified from [5-6]).

Practical methods proposed by theoretical simulation studies involving modifications of current conventional

* Corresponding author: amich18@lsu.edu

practices for enhancing multi-frac growth homogeneity. Numerical modeling performed using coupled geomechanics/fluid flow software [1], showed that at critical spacing patterns, the stress perturbation effects are balanced out and more homogeneous fracture development is promoted. These critical non-uniform cluster spacing patterns were found to yield significantly increased fracture surface area compared to uniform patterns (Fig. 2b). The results of the simulations give confidence in expanding to a laboratory-scale evaluation of non-uniform perforation cluster spacing.

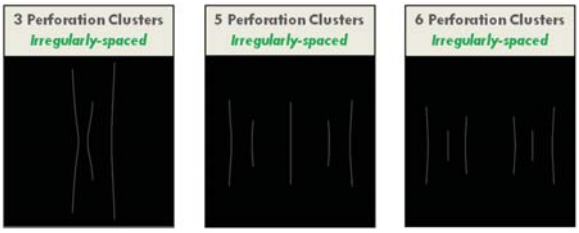

Fig. 2b. Multi-frac propagation geometries generated using *JOINTS 2.3* [4] for irregularly-spaced perforation spacing. The propagation geometries shown here for these optimized cases are much more homogeneous than the regularly-spaced patterns shown in Fig. 2a (modified from [5-6]).

2 Methods and Procedures

2.1. Laboratory Setup

The gelatin sample is cured with the aluminium "wellbore" tube inside a transparent plastic tank (Fig. 3). An overburden load (~0.2 psi) is then placed on the surface of the gelatin sample. Due to the confinement by the rigid tank walls, horizontal stresses are induced via Poisson effects, generating a normal faulting stress regime, where the overburden stress is more compressive than the two horizontal principal stresses. A piston displacement ISCO pump is used to inject fracturing fluid into the well. The fracturing fluid, initially placed in an accumulator is driven into the well by water [3].

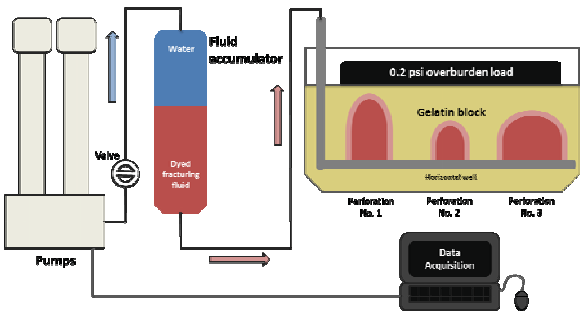

Fig. 3. Laboratory setup.

2.1.1 Reservoir Analogue Material

The reservoir analogue needed to satisfy four criteria:
- Transparent color so that fractures are visible.
- Rock-like brittleness.
- Can be easily fractured (i.e. low tensile strength).
- Low purchase price enabling multiple test runs.

Three candidate materials were selected, (i) urethane plastic, (ii) polymethyl methacrylate (PMMA), and (iii) highly-concentrated (7-8 wt. %) gelatin (Table 1). All three material candidates are transparent in color enabling good visibility of induced fracture propagation through them using dyed fluids.

Semi-circular bend (SCB) testing [7] was employed to quantify the fracture toughness, K_{IC}, of each candidate material indicating that urethane plastic's K_{IC} is too high for our purposes (i.e. it is too ductile). Then Brazilian testing was employed to assess the tensile strength, T, of the candidates indicating that PMMA's is too high to enable fracture initiation using the available laboratory equipment. This left highly-concentrated gelatin, which besides low K_{IC} (2.7×10^{-4} MPa$\sqrt{m}$) and T (in the order of 10^{-3} MPa), is also the cheapest [3] in price, as the best option to use as a reservoir analogue. Time-dependent issues were eliminated by allowing a constant cure-time.

Table 1. Preliminary testing performed on material candidates.

	Urethane plastic	**PMMA**	**Highly-concentrated gelatin**
Transparency	✓	✓	✓
Low fracture toughness, K_{IC}	×	✓	✓
Low tensile strength, T	✓	×	✓
Price affordability	×	×	✓

2.1.2 Fracturing Fluid

As for the reservoir analogue, three candidates were selected as possible fracturing fluids with viscosity being the main differentiating factor:
- Dyed water (~1 cp).
- Dyed glycerine (~74 cp).
- Dyed Vaseline® (~64,000 cp).

Pilot testing was then performed to determine which fluid can most likely generate multi-frac initiation in the highly-concentrated gelatin reservoir analogue. Dyed glycerine (Fig. 4) was found to be the best fluid option. These pilot tests were also useful for identifying optimal injection rate, q [3] for the experimental tests.

Fig. 4

Fig. 4. Pilot testing results using dyed glycerine as fracturing fluid showing multi-frac initiation.

2.2 Experimental Program

The independent variable in this experimental program is the position of Perforation No. 2 (Fig. 5); the parameter differentiating the three patterns tested (Case I, II and III). This variable is converted to a dimensionless quantity, by dividing the distance between Perforation No. 2 and No. 1 with the distance between Perforations No. 3 and No. 1, which stays constant throughout the experimental program. Hence, the "normalized position of Perforation No. 2" values for Cases I, II, III are 1/2, 2/7, and 5/7, respectively.

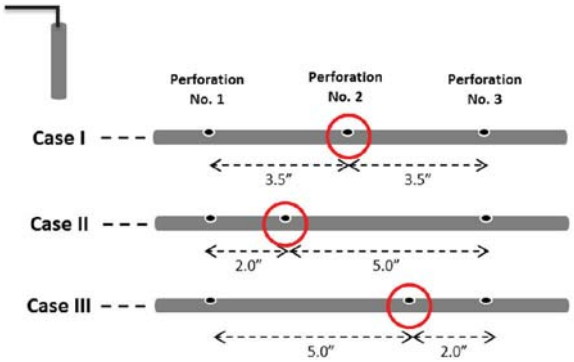

Fig. 5. The three perforation configurations used in the experimental program (modified from [3]).

2.3 Quantifying Multi-Frac Growth Homogeneity

From each experimental test, the data collected include the geometry of each induced fracture, where H_i and x_{fi} are respectively the height and length of the i^{th} fracture, while H_{max} and x_{fmax} are the corresponding height and length of the tallest and longest fracture induced in the test (Fig. 6). Each fracture height and length can be normalized by dividing the corresponding magnitude with H_{max} and x_{fmax}, respectively.

Simple analysis is performed using average mean of the normalized fracture lengths to determine the fracture length homogeneity factor (FLHF) of the resultant induced multi-frac geometry first shown in [3]. A FLHF = 1.0 represents an experimental test where all three perforations generated fractures of equal length. The minimum value FLHF can be is 1/3; which represents an experimental test where only one fracture was induced from the three perforations. Subsequently, a similar analysis is employed to calculate the fracture height homogeneity factor (FHHF) for each experimental test. Hence, the fracture geometric homogeneity index (FGHI) can be calculate as the geometric mean of FLHF and FHHF as shown below

$$FGHI = \sqrt{(FLHF \times FHHF)} \quad (1)$$

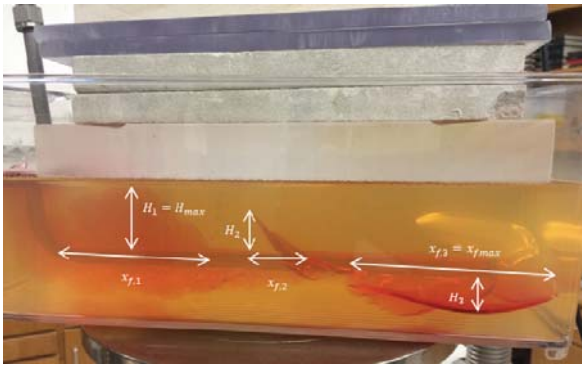

Fig. 6. Geometric parameters of the induced fractures in a laboratory test. In this test, the fracture induced from Perforation No. 1 was tallest, while the fracture induced from Perforation No. 3 was the longest.

2.4 Scaling-Up to Field Dimensions

Dimensionless groups [8] are used to compare the physics of fracture propagation in the lab tests with the field. Four dimensionless groups are used in this study:
- Experimental time, $N_t = qt/r_w^3$
- Perforation pressure drop, $N_{\Delta Pperf} = \Delta P_{perf}/E'$
- Elastic deformation, $N_{E'} = E'r_w^3/(q\mu')$
- Crack formation energy, $N_\Gamma = K_{IC}^2/(4E'^2 r_w)$

where, r_w is the wellbore diameter, t is the total injection time, ΔP_{perf} is the perforation pressure drop, $E' = E/(4–4\nu^2)$ is the "crack opening modulus" $\mu' = 12\mu$ is the channel flow viscosity [8]. Parameters from a typical cross-linked gel treatment were used for comparison purposes. For our experiments, N_t and $N_{\Delta Pperf}$ are within one order of magnitude apart from the field, which indicates good scaling, but $N_{E'}$ and N_Γ are not that close. Nevertheless, as this study addresses a problem of relative fracture propagation rather than single-frac initiation, the good proximity of N_t and $N_{\Delta Pperf}$ dominates over the not so good proximity of $N_{E'}$ and N_Γ.

Table 3. Scaling analysis.

Dimensionless group	Lab-to-field ratio	Magnitude orders apart
Experimental time	0.081	1 (good)
Perforation pressure drop	1.4	0 (excellent)
Elastic deformation	0.00032	3 (poor)
Crack formation energy	90000	5 (poor)

3 Results and Discussion

3.1 Test Results

3.1.1 Case I: Uniform Spacing

Many (four out of seven) tests resulted in one induced fracture, while several times (three out of seven) more than one fracture (Fig. 7) was induced from a single perforation.

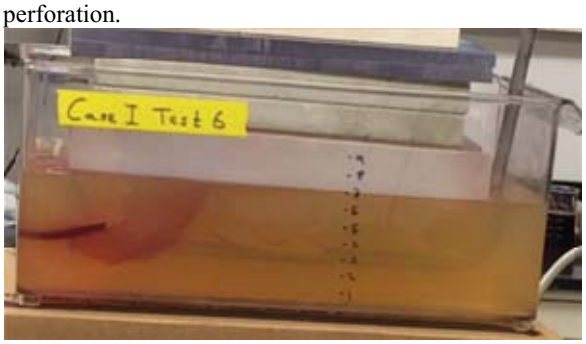

Fig. 7. A Case I test example.

3.1.2 Case II: Heel-biased Non-Uniform Spacing

This perforation configuration yielded the most consistent results compared to all the other two. Only one test led to the initiation of three fractures, while in three tests (out of seven) two fractures (Fig. 8) were observed.

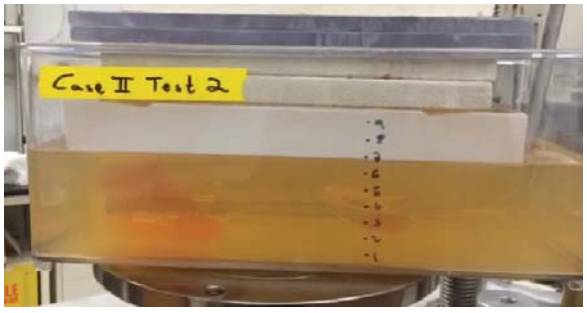

Fig. 8. A Case II test example.

3.1.3 Case III: Toe-Biased Non-Uniform Spacing

While some tests produced quite homogeneous multi-frac growth (Fig. 9a,b), this was the perforation configuration with most tests generating a single fracture (five out of seven).

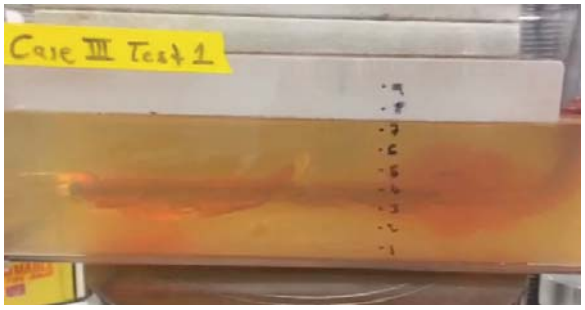

Fig. 9a

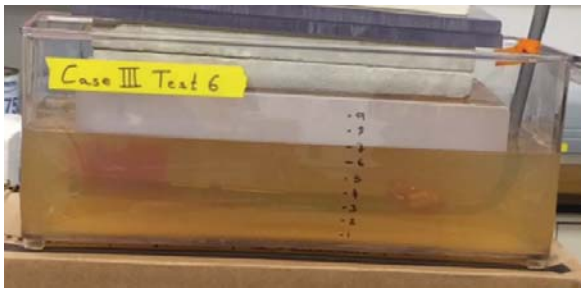

Fig. 9b. Two Case III test examples.

3.1.4 Data Analysis

The results from all 21 tests were used in the analysis. The value of FGHI (Table 2) was calculated for each test using the height and length magnitudes of all fractures induced during each test. Fig. 10 shows the variation of resultant FGHI with the position of Perforation No.2.

Table 2. Summary of FGHI results of all tests.

	Case I	**Case II**	**Case III**
Test 1	0.77	0.33	0.74
Test 2	0.71	0.51	0.33
Test 3	0.33	0.33	0.33
Test 4	0.33	0.42	0.33
Test 5	0.33	0.33	0.33
Test 6	0.71	0.49	0.55
Test 7	0.33	0.60	0.33

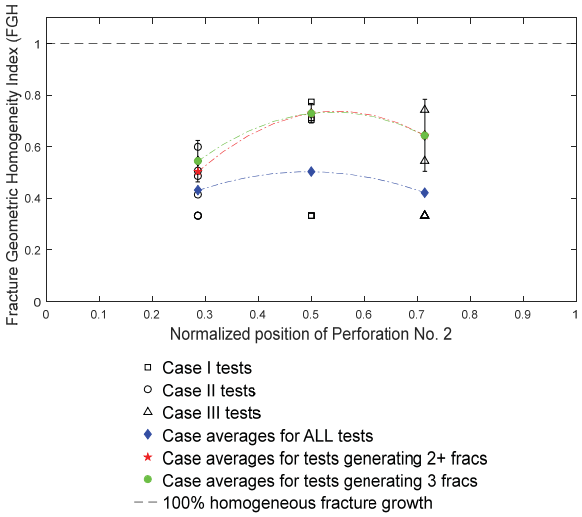

Fig. 10. Multi-frac growth homogeneity vs. perforation spacing.

3.2 Inactive Perforations

In many experimental tests perforations remained "inactive" (i.e. were unable to induce fracture initiation), while other perforations upstream and often downstream (Fig. 11) from the inactive perforation were able to induce fracture(s).

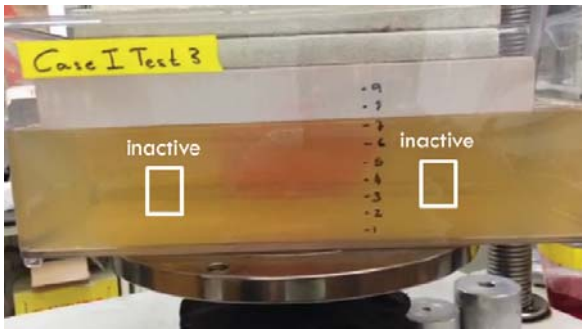

Fig. 11. Inactive perforations upstream and downstream of active perforations (modified from [3]).

This finding can be supported by logging evidence from field-scale studies [9], where clusters with no, or limited contribution to the overall production flow were observed (Fig. 12).

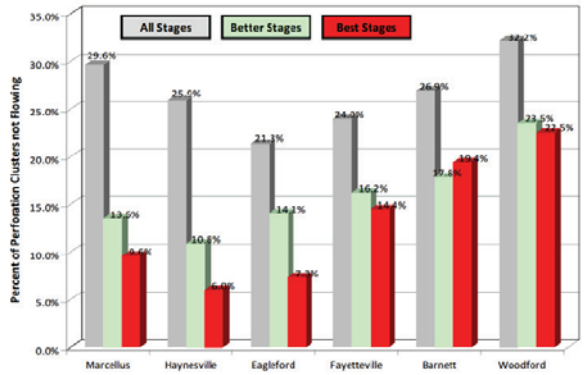

Fig. 12. Non-productive perforation clusters (from [9]).

3.3 Dominant Fractures

Another common observation from the experimental results was "dominant fracture" creation (Fig. 13). This is when by the end of the test one fracture ends up receiving the majority of the fracturing fluid resulting in those fractures dominating in size the other fractures.

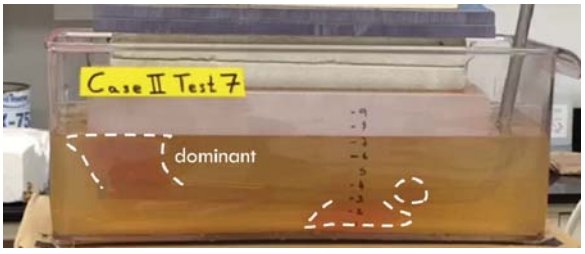

Fig. 13. Dominant fracture (modified from [3]).

Dominant fractures formed in almost every test (Fig. 13) and this finding comes in agreement real field data. Microseismic field-scale studies have supported the creation of dominant fractures even at the heel of the well (Fig. 14).

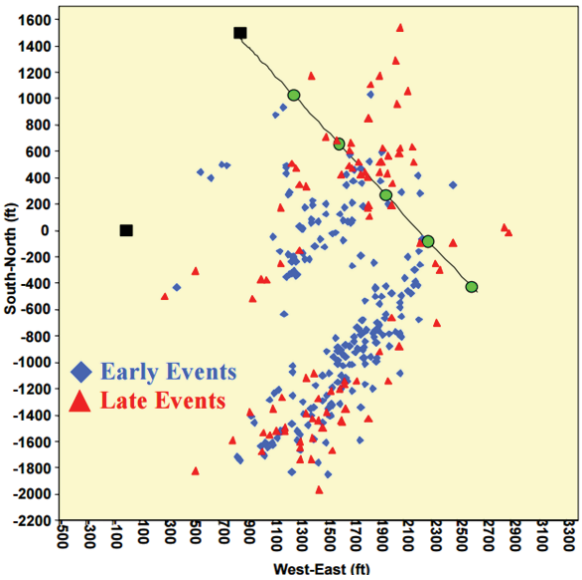

Fig. 14. Dominant fracture observation in the field (from [10]).

3.4 Probabilistic Predictive Model

3.4.1 Algorithm Framework

Monte Carlo simulation is used to generate likely scenarios of multi-frac propagation geometry by random sampling considering the available empirical data from the laboratory tests. The algorithm, which is written in MATLAB, begins by generating two random numbers from zero to one. These two numbers are used to determine arrays for the fracture lengths and the fracture heights, based on the statistical probability of occurrence of these fracture length and height (normalized) magnitudes in the laboratory tests.

The fracture height array is then rearranged, such that the relative magnitude of the elements matches the order found in the fracture height array. The assumption made is that the tallest fracture is also the longest, while the shortest is also the smallest in length. The width of each fracture is calculated using the PKN model of fracture geometry [11]. Subsequently, the fracture geometric parameters (length, height, and width) are used for plotting the predicted multi-frac propagation profiles using semi-ellipsoid shapes (Fig. 15).

For every model iteration, a curve (Fig. 16) is created indicating the predicted FGHI value as a function of the position of Perforation No. 2. The produced curve can be compared to the curve representing the laboratory data (Fig. 16). If multiple iterations are performed the average of all curves should closely match the curve from the laboratory data.

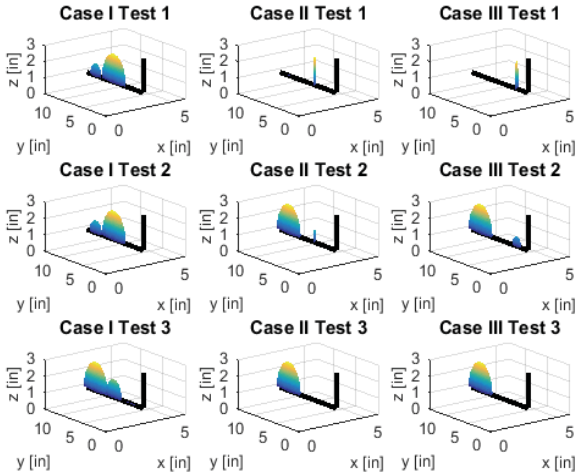

Fig. 15. The PPM uses these data inputs and Monte Carlo sampling to generate similar figures and then compare them with the laboratory results.

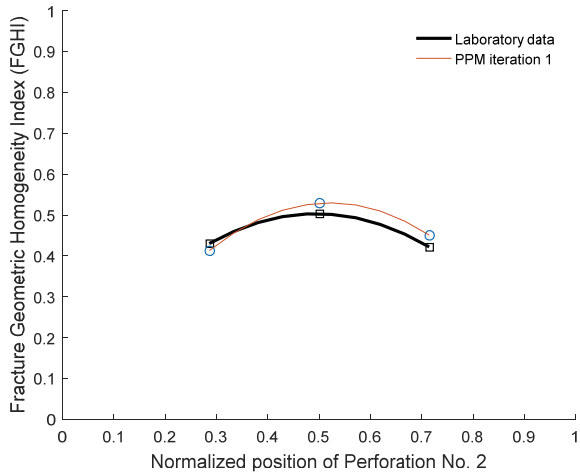

Fig. 16. An iteration example using the PPM and comparison with the empirical laboratory data.

3.4.2 Economic Impact

The PPM can be used to evaluate the induced multi-frac geometry of a fracture treatment scaled-up to field parameters. From there, the total SRV can be computed. After the fractures are generated, proppant is pumped to keep them open and provide a pathway of high permeability to the wellbore for the hydrocarbon fluids. Effective propped volume (EPV) refers to the fraction of SRV, which has been effectively propped open and is allowing flow [12-13].

Once well deliverability is modeled, the recovery from the stimulated well can be predicted. Hydrocarbon recovery projections for a given time period, over which the NPV is calculated, can be made using traditional decline curve analysis (DCA). The proppant volume, propped fracture geometry, hydraulic horsepower and other miscellaneous can be optimized using procedures, which involve amongst others the pumps pressure/flowrate constraints, maximizing fluid efficiency and proppant penetration. Fig. 17 shows the workflow for calculating the NPV of the treatment.

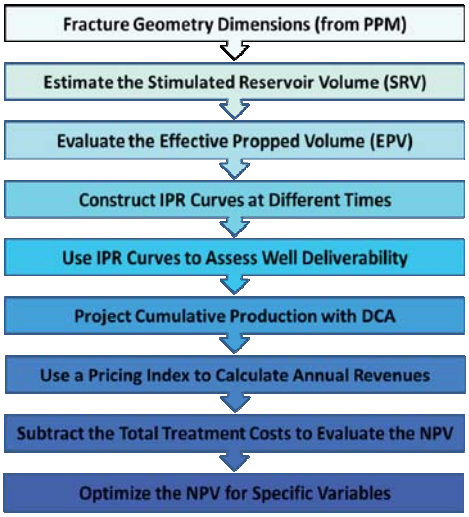

Fig. 17. Workflow for NPV calculation of a fracture treatment (modified from [13])**.**

References

1. Peirce, A., & Bunger, A. (2015). Interference Fracturing: Nonuniform Distributions of Perforation Clusters That Promote Simultaneous Growth of Multiple Hydraulic Fractures. Society of Petroleum Engineers. doi:10.2118/172500-PA
2. Michael, A. (2014). Economic Implications Of The Current Geopolitical Forces Vis-à-vis Hydrocarbons On Global Energy Markets. Society of Petroleum Engineers. doi:10.2118/169832-MS
3. Michael, A. (2016). Hydraulic Fracturing Optimization: Experimental Investigation of Multiple Fracture Growth Homogeneity via Perforation Cluster Distribution, Master's Report at the University of Texas at Austin.
4. Olson, J. E. (2008). Multi-fracture propagation modeling: Applications to hydraulic fracturing in shales and tight gas sands. American Rock Mechanics Association.
5. Mlynski, M. M. (2016). *The Effect of Perforation Spacing on Hydraulic Fracture Growth.* Poster presented for the UT PGE Summer Undergraduate Research Internship, Austin, TX.
6. Nebel, P. (2015). *Simultaneous, Multiple Fracture Growth Optimization: Laboratory-Scale Numerical Modeling.* Poster presented for the UT PGE Summer Undergraduate Research Internship, Austin, TX.
7. Chong, K.P. & Kuruppu, M.D. Int J Fract (1984) **26**: R59. https://doi.org/10.1007/BF01157555
8. De Pater, C. J., Cleary, M. P., Quinn, T. S., Barr, D. T., Johnson, D. E., & Weijers, L. (1994). Experimental Verification of Dimensional Analysis for Hydraulic Fracturing. Society of Petroleum Engineers. doi:10.2118/24994-PA
9. Miller, C. K., Waters, G. A., & Rylander, E. I. (2011). Evaluation of Production Log Data from Horizontal Wells Drilled in Organic Shales. Society of Petroleum Engineers. doi:10.2118/144326-MS
10. Fisher, M. K., Heinze, J. R., Harris, C. D., Davidson, B. M., Wright, C. A., & Dunn, K. P. (2004). Optimizing Horizontal Completion Techniques in the Barnett Shale Using Microseismic Fracture Mapping. Society of Petroleum Engineers. doi:10.2118/90051-MS
11. Nordgren, R. P. (1972). Propagation of a Vertical Hydraulic Fracture. Society of Petroleum Engineers. doi:10.2118/3009-PA
12. Balen, R. M., Mens, H.-Z., & Economides, M. J. (1988). Applications of the Net Present Value (NPV) in the Optimization of Hydraulic Fractures. Society of Petroleum Engineers. doi:10.2118/18541-MS
13. Michael, A. (2019). The Net Present Value of a Hydraulic Fracture Treatment. Society of Petroleum Engineers. *The Way Ahead*, www.spe.org/en/twa/twa-article-detail/?art=5557